Study of the Aerodynamics of a High-Speed Train Motion Under Crosswind Effect

Mohamed Aref Abdel-Mageed, Mohamed Magdy Kamal, Mohamed Adel Saad, Mohamed Adel Hamed, Tarek Youssef Abo El Yazid, Youssef Hashem El Refaey, Abdel-Rahman Mohamed Metwally
4th Year, Mech. Power Eng. Dept., Faculty of Engineering, Zagazig University, Zagazig 44519, Egypt
mohamedarefpro7@gmail.com, momagdy6899@gmail.com, mooelcicy@gmail.com, tarekaboalyazeed1999@gmail.com, abdelrahmanelgalad4@gmail.com

Supervisor: Prof. Dr. Ahmed Farouk Abdel Gawad, Prof. Dr. Mofreh Melad Nassef
Mech. Power Eng. Dept., Faculty of Engineering, Zagazig University, Zagazig 44519, Egypt
afroukgb@gmail.com, mofreh_melad@yahoo.com

Abstract: ***Modern high-speed trains' increasing velocity and decreased mass raise the topic of how severe cross winds may affect their aerodynamics. High-speed trains' running stability may be impacted by strong crosswinds due to the magnified aerodynamic forces and moments. The study of train aerodynamics under the effect of crosswind is growing with the help of various types of numerical simulation and wind tunnel. This study involved performing simulations of turbulent cross wind flows over the four cars of two simplified different models of high-speed trains at different angles of attack and different yaw angles accordingly. The train aerodynamic issues are closely associated with the flows occurring around train. The flow around the train has been considered as incompressible and was obtained by solving the incompressible form of the unsteady Reynolds-Averaged Navier-Stokes (RANS) equations combined with the SST K-ω turbulence model. Important aerodynamic coefficients such as the drag force, side force, and rolling moment coefficients have been calculated for angles of attack (0°,30°,45°,60°,90°). The results illustrated the formation of a large vortex upon the leeward side at yaw angle of 10° and above, this caused a region of low pressure which increased the overturning forces acting upon the train. Generally, crosswinds increased pressures upon the windward side of the train and decreased them upon the leeward side. Slipstream velocities on the windward side were seen to decrease whilst leeward side velocities increased. The Effect of the train shape and velocity on aerodynamic characteristics has been illustrated by comparing the results of the different cases of this study. The dependence of the flow structure on yaw angle has also been presented.***

Keywords: Cross-wind, High speed Trains, Aerodynamics, Computational fluid dynamics, K-ω turbulence model, 3D printed model.

I. INTRODUCTION

A new train trend toward faster running speeds and lighter weights has emerged in recent years in rail transportation. In regular operation, trains can travel at speeds of more than 300 km/h, which is almost as fast as light airplanes. Aerodynamic forces and moments become more significant for the train's running performance at these speeds. The running stability and riding comfort of the vehicle may be affected by strong crosswinds. The increase of the aerodynamic forces and moments because of crosswind may influence the train operating safety and the worst case may lead train to overturn [1]. The risk of crosswind that may cause train to overturn depends on the track infrastructure and vehicle aerodynamics. The number of accidents involving trains overturning has increased due to the track infrastructure's exposure to strong crosswinds and unexpected wind gusts, which includes tall viaducts and high embankments. On the other hand, aerodynamics, particularly on the leading car, plays a significant role in train stability when subjected to strong crosswinds. The leading car is the most sensitive because it is exposed to the greatest aerodynamic loads [1].

A. History

The first crosswind-related train overturning occurred in St. Louis, United States of America, in April 1882 when a passenger train was blown off a narrow gauge track during a severe storm. Since then, there have been a total of 29 crosswind-related accidents, the majority of which have occurred in Japan as a result of the country's narrow gauge lines. The BART line (Bay Area Rapid Transit, San Francisco, USA) chose broad gauges, which are 17% wider than standard ones, to improve train stability for crosswinds and earthquakes. Accidents caused by wind have been recorded involving both passenger and freight trains on standard gauge tracks in high-risk locations, such as bridges and embankments. The Lanzhou-Xinjiang High Speed Railway, for instance, travels through a plain desert region in China that is constantly blown by strong winds. During a sandstorm in 2007, wind gusts caused an 11-car train to flip over. Figure (1) shows other recent examples of train overturning due to strong crosswinds: two light trains in

Europe (Austria, 2002 and Switzerland, 2007) and a locomotive in Japan (2006) [2].

Fig. 1: Crosswind related accidents.

B. *Crosswind*

As soon as a train moves through windy conditions, crosswind happens. The relative wind that loads the train is produced when the wind and train velocity combine. This aerodynamic load has the potential to be powerful enough to turn the train around. As the number of high-speed lines in Europe has drastically increased over the past few decades, crosswind stability of high-speed trains has gained more attention. Overturning a high-speed train at 300 km/h would have deadly consequences. As the relative velocity between the side wind and train increases, so does the strength of aerodynamic loads, increasing the risk of an accident. In figure (2), the definition of train traveling under a crosswind condition is presented. The relative wind velocity V is the velocity between the train traveling speed v and the wind velocity u. The yaw angle ψ is defined as the angle between the relative velocity and the train velocity and the wind angle of attack β between the train wind velocities [2].

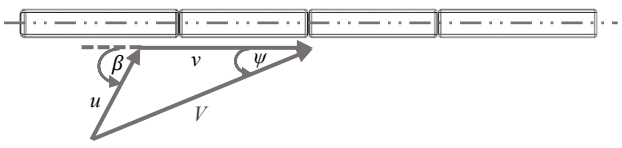

Fig. 2: Components of natural wind velocity relative to the train.

C. *The cases of the study*

In this study, we have three cases with two different models at five angles of attack. Table (I) illustrates the three cases which includes the train types, velocities, crosswind velocity and its classification.

TABLE II
THE DIFFERENT CASES OF THIS STUDY

Cases	Case (1)	Case (2)	Case (3)
Train Type	Aerodynamic Train	Ordinary Train	Aerodynamic Train
Train Velocity	100 Km/h	100 Km/h	200 Km/h
Crosswind Velocity	13 m/s = 46.8 Km/h	13 m/s = 46.8 Km/h	14 m/s = 50.4 Km/h
Crosswind Type	Strong Breeze Range: (39-49) Km/h	Strong Breeze Range: (39-49) Km/h	High Wind OR Near Gale Range: (50-61) Km/h

As shown in the following figures, we have two models one of them is a simplified aerodynamic model of The Stadler EC250 (Giruno) and the other is a simplified ordinary one of (Henschel). The two models have the same dimensions, velocities and exposed to the same crosswind conditions. The aerodynamic model is considered to be as a modification of the ordinary one to improve the aerodynamic characteristics.

(a) (Giruno) (b) (Henschel)

Fig. 3: Aerodynamic shape (a), Ordinary shape(b).

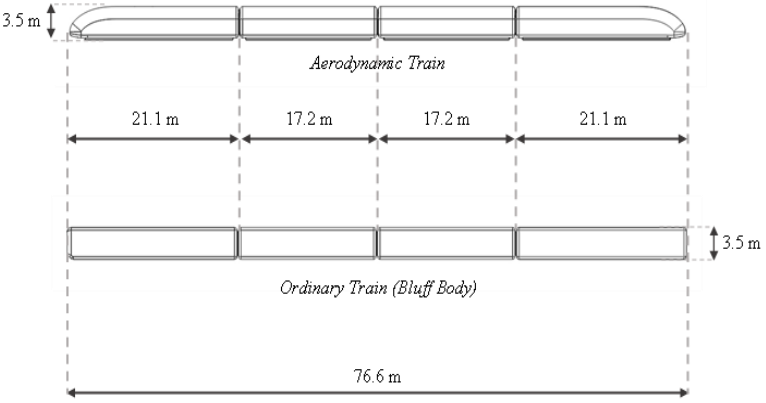

Fig. 4: Schematic of our study two models.

D. *Objectives*

The aim of this study is:

(a) Improving safety in high-speed trains under the influence of cross winds.
(b) Study the effect of train shape and velocity on aerodynamic characteristics.

(c) Understanding the flow nature around the trains.
(d) Explaining the effects of velocity and pressure on and around the trains.
(e) Illustrating the vortices in leeward side.
(f) Comparing The resultant force of drag and side for the three cases.
(g) Validating the numerical value of drag coefficient at angle zero for the aerodynamic train by comparing it to the experimental one.

II. Literature Review

If the parameters in the equations are known, numerical solutions to differential equations can be obtained using a variety of methods. Analytical solutions to mathematically defined problems are possible, but time consuming, and the approximation error obtained differs from the numerical solution. In the past, a variety of research on train aerodynamics was performed using numerical simulation and experiments. Although previous experimental analysis focused on the train's effect on the crosswind, flow physics has not been a priority concern [3].

An accurate way to produce absolute values of the measured aerodynamic loads is through experimental investigation, which is both reliable and acceptable. It is clear that over the past few decades, experimental research has risen to the top as a preferred method of gathering important information about train aerodynamic phenomena. On the other hand, the accuracy of numerical results has historically been contested. However, the computational simulation approach has gained a lot of popularity recently. Computational fluid dynamics (CFD) has potential in the field of vehicle aerodynamics as the capacity of contemporary computational resources, i.e., high-performance computers, grows [3].

A. *Aerodynamics analysis on the train*

Due to the flow pressure and the local pressure changes, three forces and moments are generated on the train as shown in the following figure.

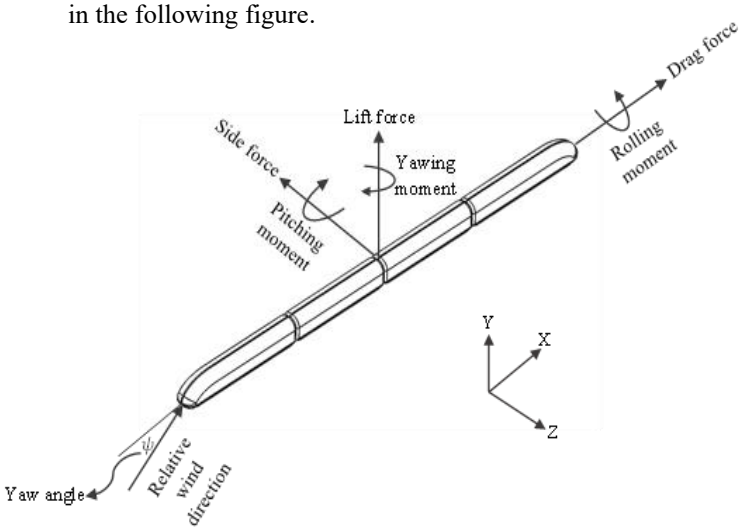

Fig. 5: Aerodynamic forces and moments.

TABLE III
AERODYNAMIC LOADS DEFINITION

Drag Force	The Force that the air flow exerts on the train in the flow direction (X direction).
Side Force	The generated force on the train side in (-ve) Z direction by air flow.
Lift Force	The Force that is perpendicular to the flow direction (Y direction).
Rolling Moment	The generated moment about the flow direction (Drag Direction).
Pitching Moment	The generated moment about the force side direction.
Yawing Moment	The generated moment about the lift direction.

The non-dimensional aerodynamic forces and moments coefficients can be expressed as:

- Drag force coefficient:

$$C_d = \frac{F_d}{0.5\rho V^2 A_d} \quad (1)$$

- Side force coefficient:

$$C_s = \frac{F_s}{0.5\rho V^2 A_s} \quad (2)$$

- Lift force coefficient:

$$C_l = \frac{F_l}{0.5\rho V^2 A_l} \quad (3)$$

- Rolling moment coefficient:

$$C_{MR} = \frac{M_x}{0.5\rho V^2 w^2 l} \quad (4)$$

- Pitching moment coefficient:

$$C_{MP} = \frac{M_z}{0.5\rho V^2 l^2 w} \quad (5)$$

- Yawing moment coefficient:

$$C_{MY} = \frac{M_y}{0.5\rho V^2 l^2 h} \quad (6)$$

Where: F_d: drag force, F_s: side force, F_l: lift force, A_d: the projected area in x direction, A_s: the projected area in - z direction, A_l: the projected area in y direction, M_x: rolling moment, M_z: pitching moment, M_y: yawing moment, w: train width h: train height l: train length V: relative wind velocity, ρ: flow density.

B. *Velocity analysis*

The magnitude of a train's aerodynamic loads is affected by the direction of the effective crosswind. In this case, the effective crosswind is defined as the vector summation between the train speed (**v**) and the wind velocity (**u**) as shown in Figure (6) [4].

We can calculate relative wind velocity (V) and Yaw angle (ψ) as following:

$$V^2 = [v + u\cos(\beta)]^2 + [u\sin(\beta)]^2 \quad (7)$$

$$\tan(\psi) = \frac{u\sin(\beta)}{v + u\cos(\beta)} \quad (8)$$

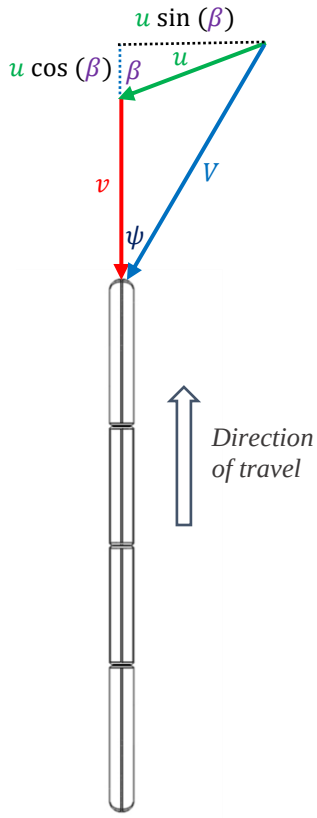

Fig. 6: Velocity analysis schematic.

III. METHODOLOGY

In this study, we have two methodologies to understand the flow nature around the trains, first of them is computational or numerical methodology and the second is experimental one. Computational Fluid Dynamics (CFD) was used to study the flow around the high-speed trains (HST) under crosswind effect. The flow was simulated with the commercial CFD software solver ANSYS FLUENT Version R19.2 on a full-scale model (head car, tail car and two middle cars). The flow around the train has been considered as incompressible and is obtained by solving the incompressible form of the URANS equation combined with the help of turbulent model [K-ω (SST)]. Experimental measurements were performed in wind tunnel on only one 3D printed head car with scale of 1:87.5.

A. *Governing Equations*

The equations which govern the flow over the train are the continuity and Navier–Stokes equations. The flow around the train in our particular problem is assumed to be incompressible. Hence, for turbulent flow, the incompressible unsteady RANS equations can be written as:

$$\frac{\partial(\rho\overline{u_\iota})}{\partial x_i} = 0 \tag{10}$$

$$\frac{\partial \rho\overline{u_\iota}\overline{u_j}}{\partial x_i} = -\frac{\partial}{\partial x_i} + \frac{\partial \bar{p}}{\partial x_j}\left[\mu\left(\frac{\partial \overline{u_\iota}}{\partial x_j}\right) - \rho\overline{\acute{u}_\iota\acute{u}_j}\right] \tag{11}$$

Where $\overline{u_\iota}$ are the averaged velocity components and $\acute{u}_\iota$ the fluctuation components, ρ the flow density, μ the dynamic viscosity and $\bar{p}$ the averaged pressure. Time-averaging introduces the tensor $-\overline{\acute{u}_\iota\acute{u}_j}$ known as the Reynolds-stress tensor.

For three-dimensional flows the four equations involve ten unknowns, $\bar{p}$, $\overline{u_1}$, $\overline{u_2}$, $\overline{u_3}$ and the six Reynolds-stresses components. To close the system, the Reynolds-stress tensor is superseded by turbulence models [5].

B. *Computational solution steps*

In this aspect, the steps of performing the simulations in ANSYS FLUENT will be explained. The first step is by creating the model geometry in commercial CAD software SOLIDWORKS. Then, the model is exported to Design Modeler and the computational domain is created. Next, the meshing process is performed.

The physical Properties is defined for the external domain. An unstructured tetrahedrons mesh was used for this domain. In the process of meshing, the position of inlet, outlet, symmetry and wall of the model is also defined.

After the process of meshing completed, the solver Type, the time, the boundary conditions of the model, the turbulence model, the type of flow, the solution methods, and the report definition for aerodynamic forces and moments must be set in the setup process. Then, the simulation is run and data are collected and analyzed.

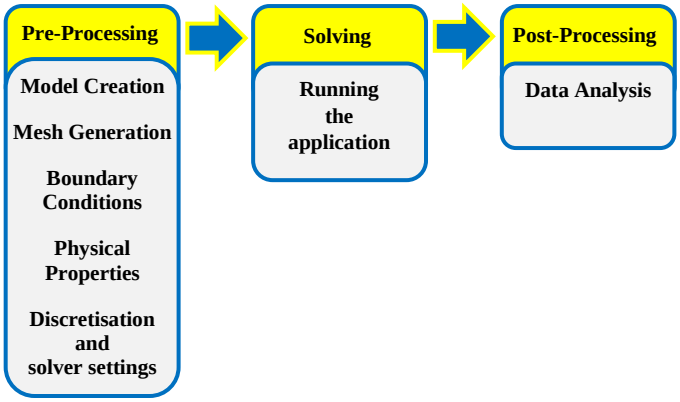

Fig. 7: Steps in performing simulation in ANSYS.

1. Geometry model

The models were established in full-scale dimensions. In order to capture the real flow field around train and minimize the boundary effect in crosswinds.

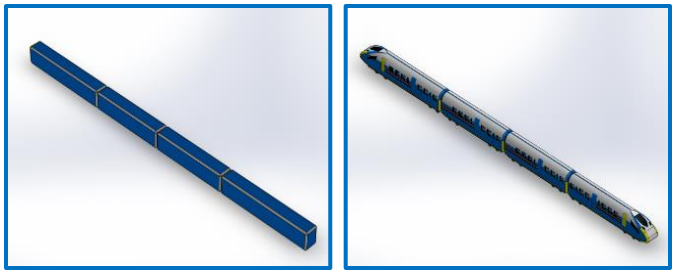

Fig. 8: The design of the ordinary and aerodynamic train models in SOLIDWORKS.

We have designed the models in commercial CAD software SOLIDWORKS as shown in figure (8), then the models were exported to Design Modeler in ANSYS.

The Configurations and Dimensions of the train models will be illustrated in the following figures and table.

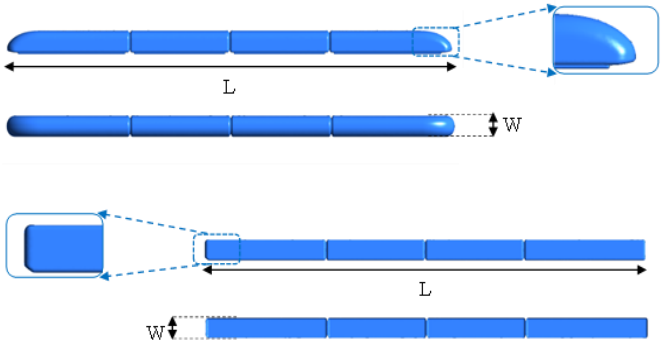

Fig. 9: Side and top views of the two models.

Fig 10: Front view of the two models.

In figure (11), the modification of the ordinary train to be an aerodynamic one with more curved and streamlined edges, corners and nose.

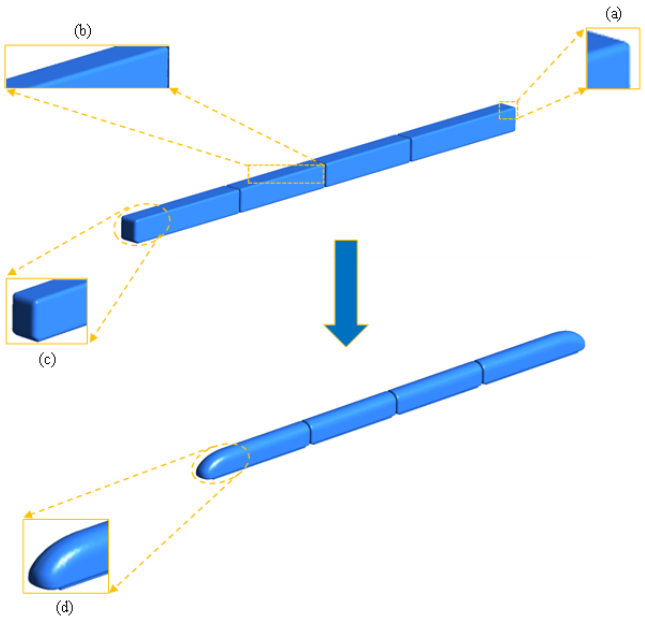

Fig. 11: The isometric view of the model before and after modification. (a), (b) are a close view of the nearly sharp corners and edges respectively, which are modified to be more curved and streamlined. (c), (d) are the shapes of nose before and after modification

TABLE IV
THE DIMENSIONS OF THE GEOMETRIC MODELS

Dimension	Value
Length (L)	76.6 m
Width (W)	3 m
Height (H)	3.5 m

2. Computational domain

CFD simulations are performed on a fluid computational domain. The computational domain dimensions for the two different models are (176.6 m×73 m×23.7m). After the domain was created, the train was extracted from it by Boolean.

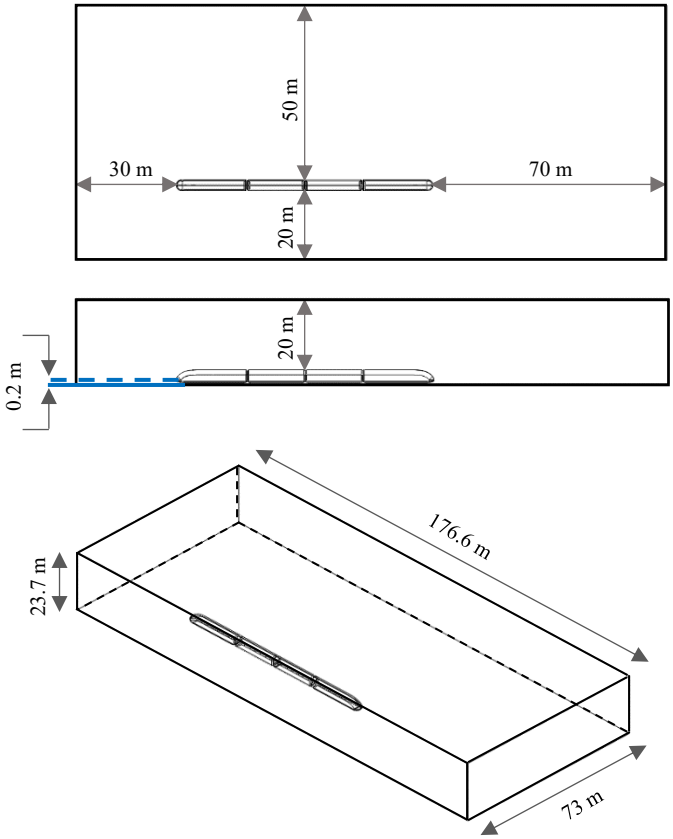

Fig. 12: Computational domain dimensions and the train position.

3. Mesh Process

The mesh of the computational domain was generated using a tetrahedron patch conforming method. Mesh refinement has been done on the train surfaces, bogies of the train and areas surrounding the train. The body sizing was performed with an element size of 1 m for the two trains, capture curvature and capture proximity are also activated. The inflation was generated around the train body to catch the flow details with ten layers, a transition ratio of 0.272 and a growth rate of 1.2.

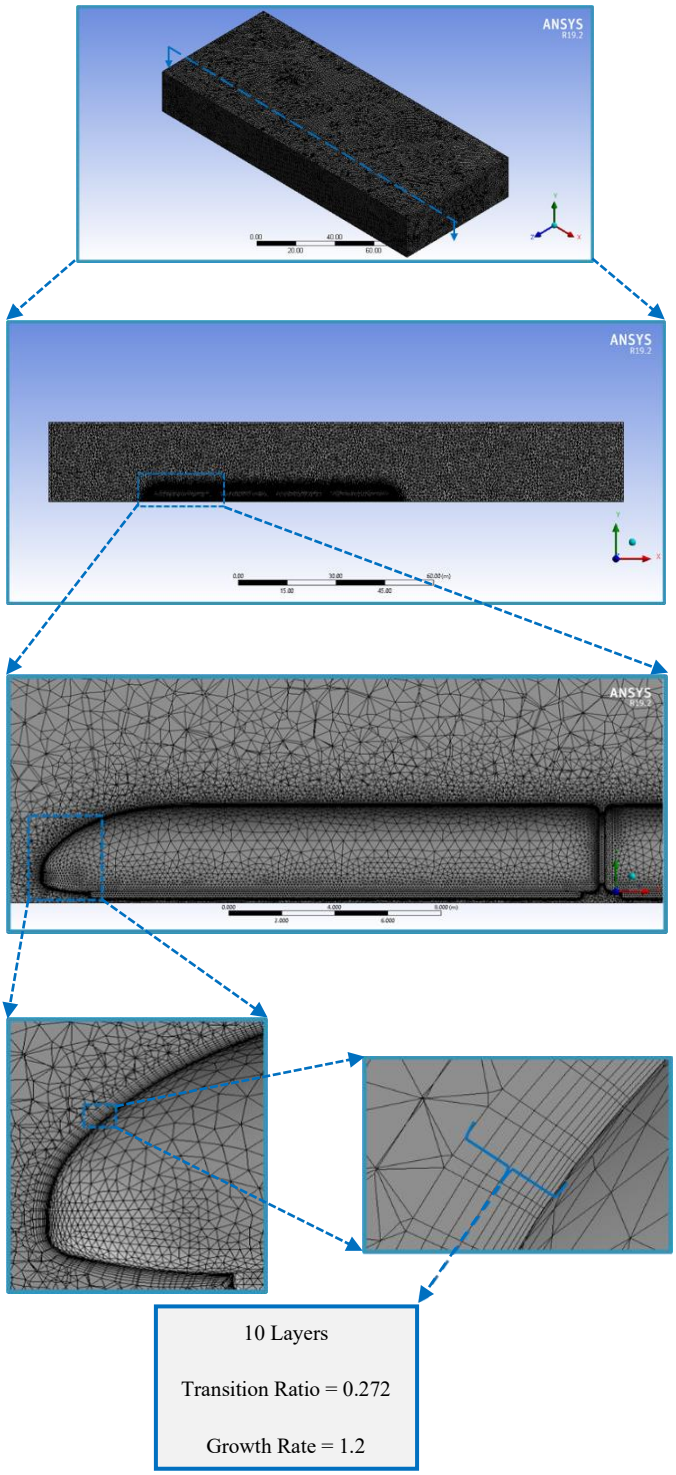

Fig. 13: A cross section illustrates mesh generation and inflation around the train.

The generated mesh consists of 4541845 elements for aerodynamic train and 4852242 elements for ordinary train. In this process, the position of inlet, outlet, symmetry, and wall of the model is also defined.

4. Boundary conditions and solver settings

The flow enters the domain with a variable velocity based on each case and each angle. The Reynolds Number based on the various inlet flow velocity the width and the length of train model (Characteristic length) was ranging between minimum value of 5.1418×10^6 and maximum value of 2.9775×10^8.

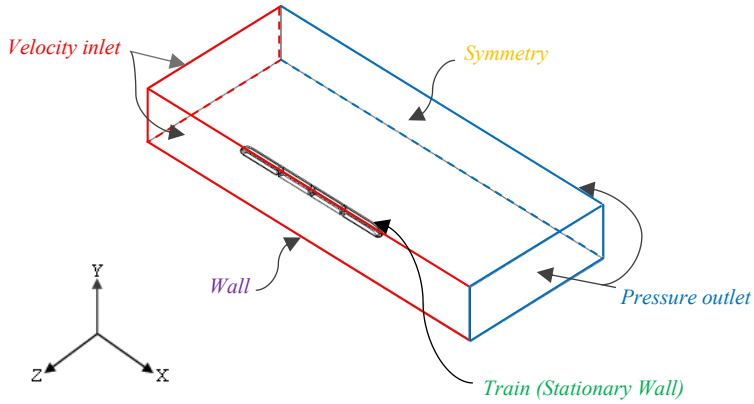

Fig. 14: Boundary conditions used in numerical investigation.

TABLE V
SOLUTION SETUP STEPS

Solver	Pressure based & Transient and Steady
Turbulent Model	K-ω (SST)
Flow type	External flow (Air)
Inlet-velocity	Components of the relative velocity in X & Z direction
Outlet-pressure	0 Pa (Neumann boundary)
Wall	Stationery wall
Pressure-velocity coupling (Scheme)	Simple
Momentum	Second order upwind
Report definitions	Drag & Side & Lift Forces Rolling moment
Initialization method	Standard Initialization
Time step	0.01 sec
Number of time steps	5000-6000

C. *Experimental solution*

The tests were carried in our Department of Power Mechanical Engineering Laboratory. The experimental model is a 3D printed model of the Cad model that was designed in SOLIDWORKS. We printed only one head car with a scale of 1:87.5 from the full-scale numerical model because of the lack of possibilities.

The model was attached to a calibrated spring and was installed on a moving slider then, the train with the slider was well installed on wind tunnel. We measured the length of the attached spring before the model being subjected to the air flow then, the centrifugal fan was turned on, the flow moved the slider back, and the spring stretched with a displacement.

Fig. 15: Wind tunnel and the test section.

The dimensions of the test section are: 27 cm * 27 cm * 90 cm. The velocity of the air flow is 22 m/s.

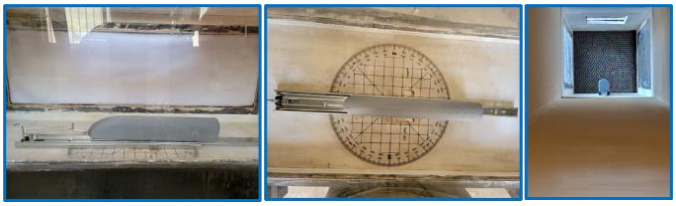

Fig. 16: The 3D printed model in test section from different views.

The dimensions of the model are 24 cm * 3.5 cm * 4 cm. The frontal area of the model is 11.7257 cm^2. The new length of the spring was measured after stretching and the displacement was calculated by subtracting the original length from the new length. The drag force at angle zero was calculated by multiplying the stiffness of the spring by the displacement then the drag coefficient was calculated.

$$C_d = 0.479$$

IV. Results and Discussion

After the simulation was done, the data were collected to be analyzed and this is what is known as post-processing. We have so many results to explain in this section so we will show some of them in some cases and all of them in some other cases.

A. *Velocity contours*

The velocity contours are inverted as to represent a moving train rather than that of a stationary train in a moving flow. We will just show the velocity contours for case (1) in which the train is an aerodynamic one, v=100 Km/h, u=13 m/s, and the five angles are 0°, 30°, 45°, 60°, 90°.

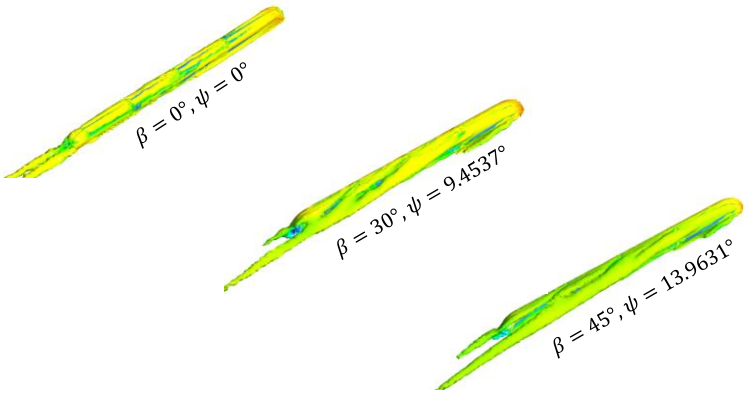

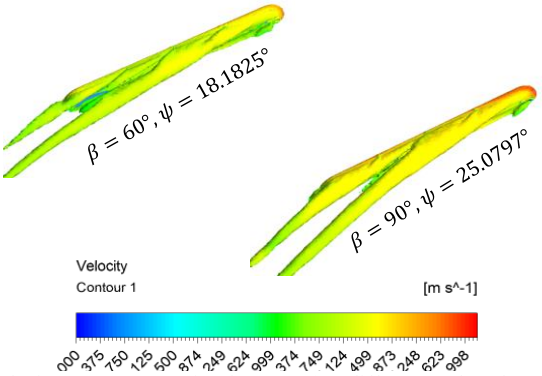

Fig. 17: Velocity vortex core region for case (1) at different angles of attack and Yaw angles.

When the air flow attacks the train body, a stagnation point is generated. At stagnation point, the velocity is zero and the pressure is maximum. When the angle of attack increases the Yaw angle increases so that the separation of the flow structure increases far from the train body.

B. *Pressure contours*

The train body exerts different pressure on the approaching wind flow with the particular pressure range because of the differences in the direction of the wind flow. Normally, the mean pressure contour will involve the relationship between the pressure and the velocity. Based on Bernoulli's Principle, as the velocity increases, the pressure will steadily decrease.

1. Pressure contours on the front of the trains, windward side and leeward side

In the following figures, for cases (1) and (2) at $\beta = 0°$, the pressure is steadily exerted on the frontal surface of the train model. The red color for the mean pressure indicates that the frontal surface has the highest pressure because the direction of inlet velocity flows directly to the frontal surface.

At $\beta = 30° and\ \beta = 45°$, it is obvious that the low-pressure region on the windward surface begins to shrink and spread on the leeward surface because of the existence of wind resultant velocity. The critical condition of pressure remains the same at the frontal surface but slowly takes place to the windward side surface.

At $\beta = 60°$, the critical condition that indicates the higher pressure started to increase at the side view (windward) due to the existence of increasing crosswind's angle.

The pressure exerted on the frontal surface significantly decreases but it substantially increases for side surface(windward) for the crosswind at $\beta = 90°$.

For case (3), what occurs in cases (1) and (2) at angle $\beta = 45°$, in this case occurs at $\beta = 90°$ as the maximum Yaw angle in cases (1) and (2) equals $\psi = 25.0797°$, but in case (3) equals $\psi = 14.1441°$.

In cases (1), (2) at $\beta = 45°$ Yaw angle equals $\psi = 13.9631°$. Pressure contours will be shown on the front of the trains for all cases and on windward side and leeward side for case (1), (2) only.

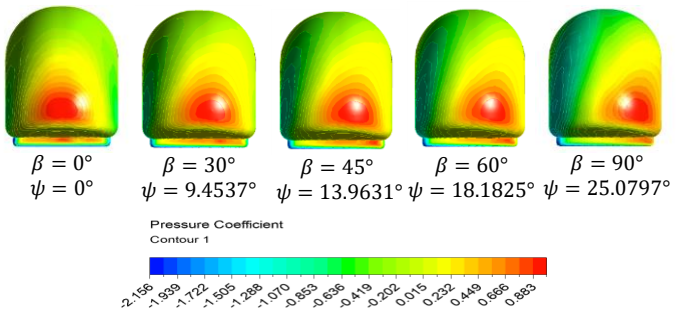

Fig. 18: pressure distribution on the front of the trains and pressure coefficient for case (1).

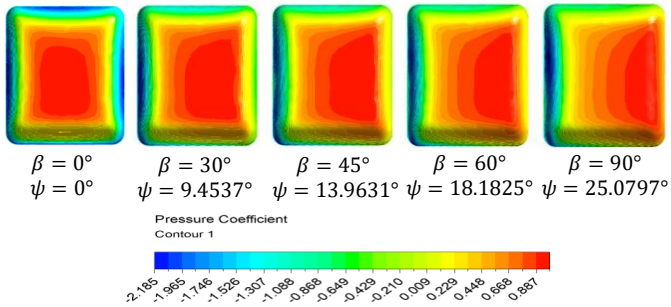

Fig. 19: pressure distribution on the front of the trains and pressure coefficient for case (2).

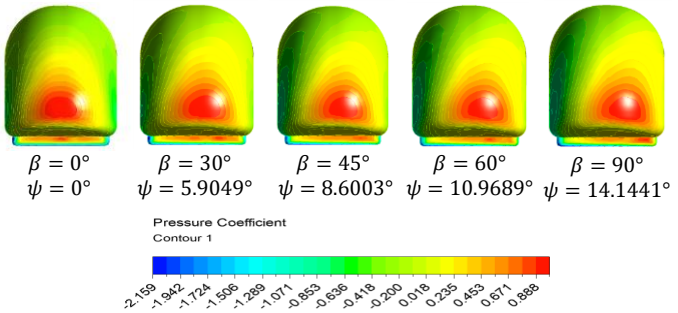

Fig. 20: pressure distribution on the front of the trains and pressure coefficient for case (3).

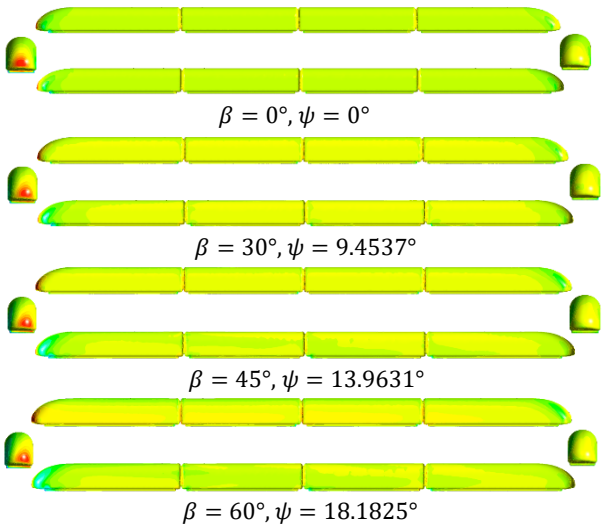

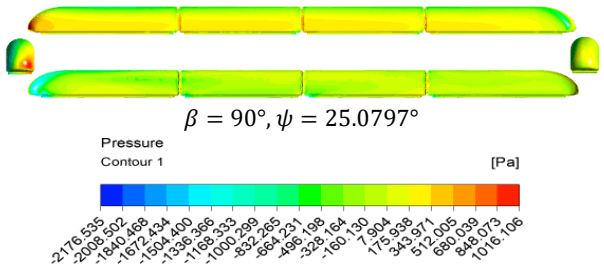

Fig 21: Pressure distribution on windward side and leeward side respectively for case (1) at all angles.

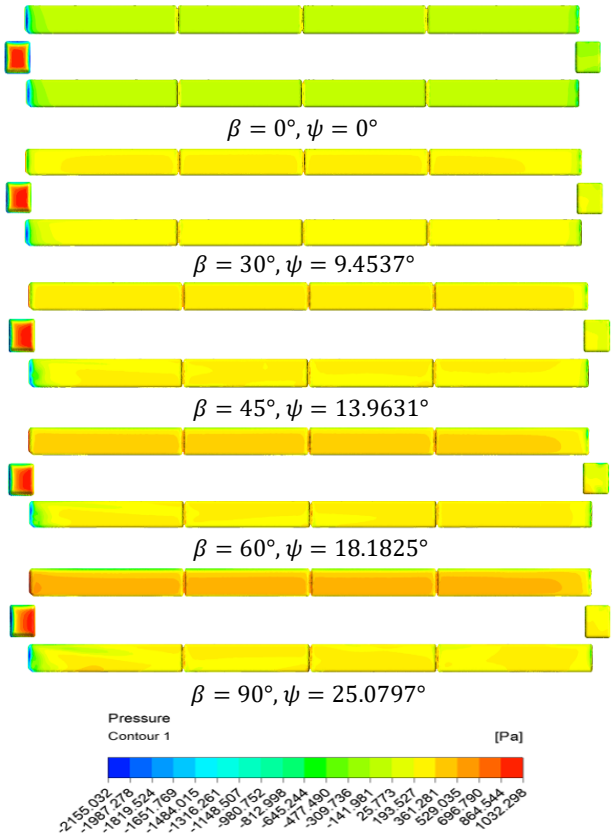

Fig. 22: Pressure distribution on windward side and leeward side respectively for case (2) at all angles.

From the previous figures, it is obvious that the pressure generated on the ordinary train is higher than the one generated on the aerodynamic train and also the pressure losses in leeward side is higher for the ordinary train because of sharp corners, edges and the bluff shape of the nose which indicates that the forces that will be generated on the front and side of this train will be higher than the ones generated on the aerodynamic train. The vortices will be also large in size in case of the ordinary train.

C. Streamlines

The flow separation takes place on both the lower and upper leeward edges and the vortex distribution depends on the yaw angle. The recirculation region caused by the vortex flow starts being adjacent to the walls of the train, then it slowly

drifts away from the surface as the flow develops further towards the wake. These vortices develop into larger size as the yaw angle increase. The presence of vortex on the leeward side formed the region of low pressure at the leeward. As the vortex larger in size, the pressure is decreased and hence increase the side force on the windward side

1. Surface streamlines (vortices illustration)

The flow structure for different yaw angles is shown in detail by the two-dimensional streamlines at different cross sections along the train length.

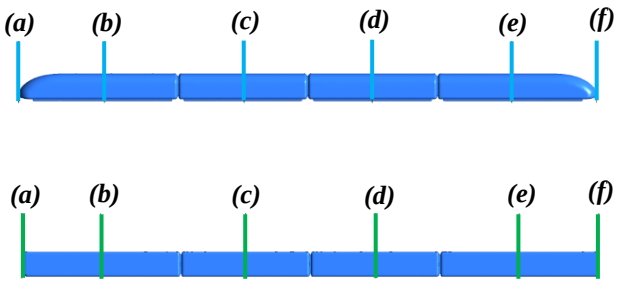

Fig. 23: The location of the cross sections on which, streamlines are illustrated.

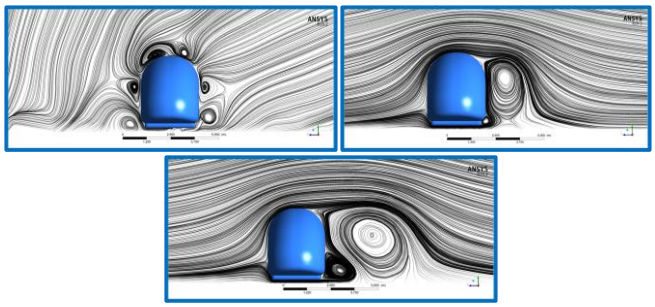

Fig. 24: Vortices variation for the same case (1), on the same cross section (C), at different Angles of attack: (0, 45, 90).

As we see in figure (24), at the same location on the train, when the angle of attack increases and accordingly Yaw angle, the flow separation increases and the vortices size increases.

In the following figures streamlines will be illustrated on the six cross sections along the train length for case (1), (2) and (3) respectively at angle $\beta = 90°$.

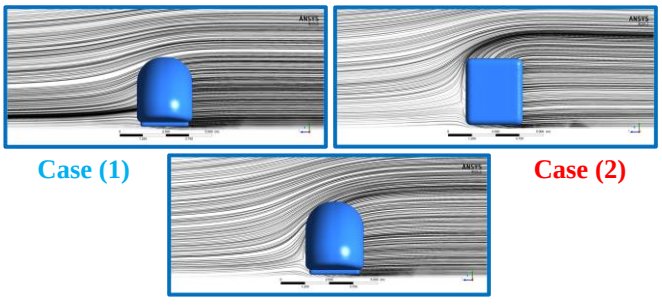

Fig. 25: Streamlines on the cross section (a) for the three cases at $\beta = 90°$.

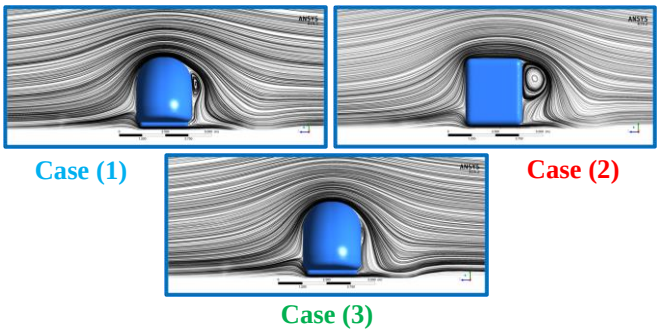

Fig. 26: Streamlines on the cross section (b) for the three cases at $\beta = 90°$.

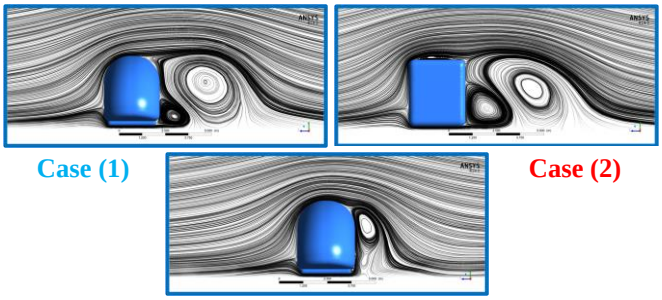

Fig. 27: Streamlines on the cross section (c) for the three cases at $\beta = 90°$.

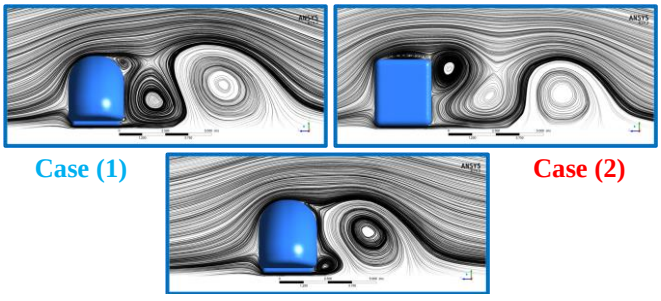

Fig. 28: Streamlines on the cross section (d) for the three cases at $\beta = 90°$.

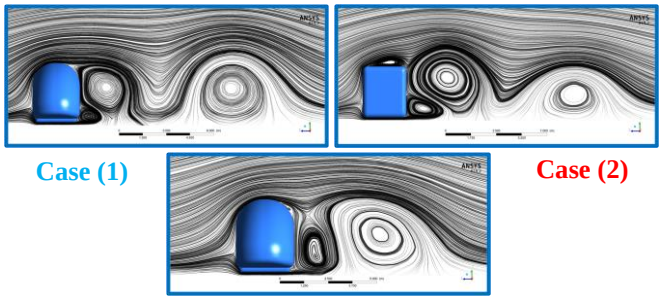

Fig. 29: Streamlines on the cross section (e) for the three cases at $\beta = 90°$.

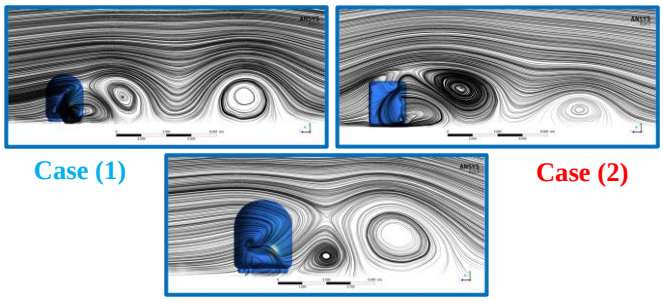

Fig. 30: Streamlines on the cross section (f) for the three cases at $\beta = 90°$.

2. 3D streamlines

In figure (31), 3D streamlines are illustrated to show more details of flow structure.

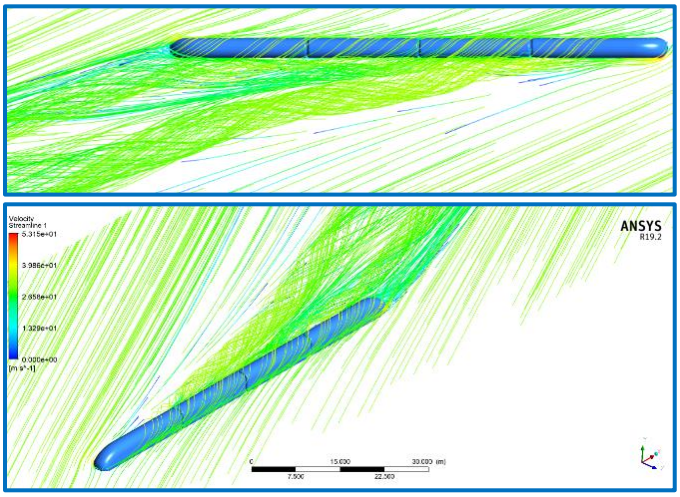

Fig. 31: 3D streamlines from some views to illustrate the flow structure details.

D. Aerodynamics loads

The date of forces and moments were collected and scheduled in tables then, converted into graphs to be compared and analyzed. The validation is performed at zero angle for drag force for case (1) by comparing the numerical data by the experimental one.

1. Drag force

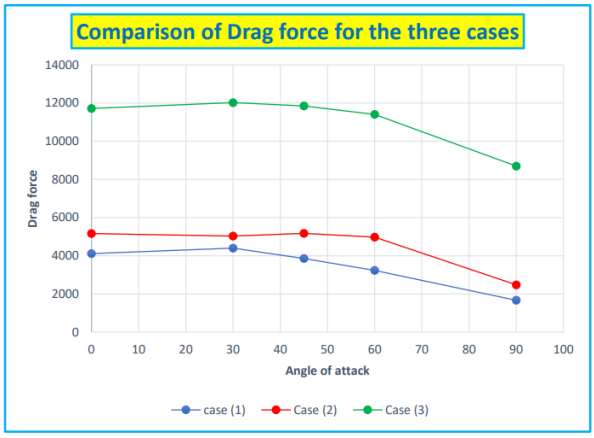

Fig. 32: Comparison of the drag force for the three cases at different angles of attack.

As shown in figure (32), the drag force values for case (3) are the highest ones because of the high velocities in this case compared to case (1) and (2) where, the drag force is proportional to wind relative velocity. The drag force values for case (2), is higher than case (1) which indicates that the aerodynamic train design decreases the drag force compared to the ordinary one at the same dimensions and the same angles of attack. It is obvious that the highest drag force for cases (1) and (3) is at $\beta = 30°$ and for case (3) at $\beta = 45°$.

2. Side force

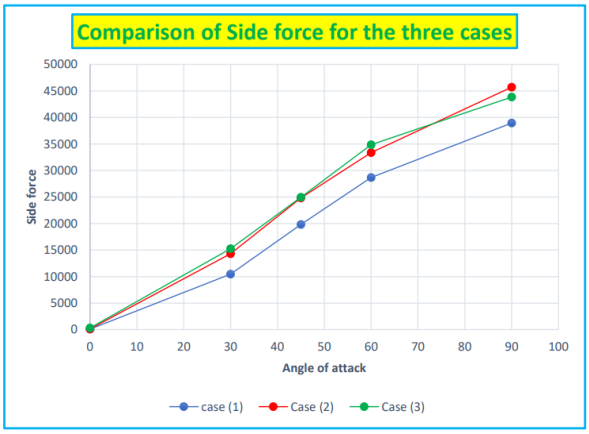

Fig. 33: Comparison of the side force for the three cases at different angles of attack.

As shown in the previous figure, the values of side force, is the highest for case (3) at all angles except $\beta = 90°$, the side force of case (2) is the highest at this angle. The side force values for case (2), is higher than ones of case (1) which indicates that the aerodynamic train design decreases the side force compared to the ordinary one at the same dimensions and the same angles of attack. The side force values of case (2), is very close to the ones of case (3), despite the large velocities difference between them.

3. The resultant force of drag and side

The following figure provides a comparison of the resultant force (Drag & Side) for the three cases at the same angles of attack which is the main objective of this study. This graph illustrates the effect of shape and velocity on the resultant force which case (3) has the highest values compared to the two other cases because of the increasing in velocity and case (2) is higher than case (1) which indicates that the generated forces on the ordinary train are higher than the aerodynamic one due to the bluff body shape.

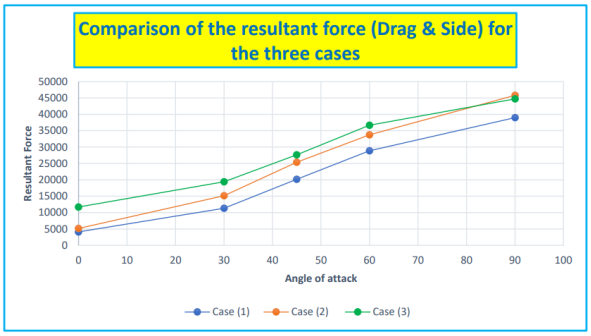

Fig. 34: Comparison of the resultant force for the three cases at different angles of attack.

4. Rolling moment

The rolling moment is the result of both the lift and side forces with the side force being the main contributor. The rolling moment is responsible for the overloading of wheel-track on the leeward side and is found to be one of the most

important aerodynamic coefficients regarding cross-wind stability.

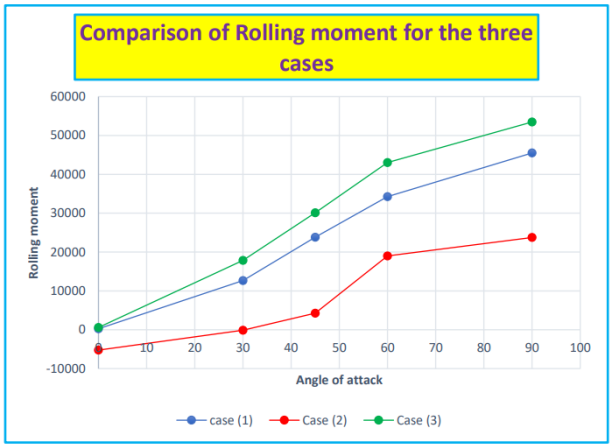

Fig. 35: Comparison of the rolling moment for the three cases at different angles of attack.

E. Validation

The drag force at angle zero was calculated by the spring stiffness and displacement and it was 0.1666 N. To perform validation the numerical drag coefficient at zero angle must be compared to the experimental drag coefficient at the same angle so we calculated the drag coefficient and it equals 0.4793.

TABLE VI
THE VALIDATION OF DRAG COEFFICIENT

	Drag Coefficient		
Yaw angle	Numerical	Experimental	Error
0°	0.393	0.4793	18%

The error is due to the scale of the model and the friction of the slider.

V. Conclusion

The aim of the research within this thesis was to provide an improved understanding of the aerodynamic characteristics of a high-speed passenger train and how these characteristics are affected by crosswinds at different yaw angles.

The flow of turbulent crosswind over the two high-speed train models has been simulated numerically by solving the unsteady three-dimensional RANS equations. The simulation has been done in stationary ground case for three cases and at different yaw angles and angles of attack (0°,30°,45°,60°,90°). The computed aerodynamic coefficient outcomes using the SST K-ω turbulence model were in good agreement with the wind tunnel data for one case and one angle.

The drag force values for case (3) are the highest ones because of the high velocities in this case compared to case (1) and (2) where, the drag force is proportional to wind relative velocity. The drag force values for case (2), is higher than case (1) which indicates that the aerodynamic train design decreases the drag force compared to the ordinary one at the same dimensions and the same angles of attack. It is obvious that the highest drag force for cases (1) and (3) is at β=30° and for case (2) at β= 45°.

Both the side force coefficient and rolling moment coefficients increase steadily with yaw angle for the three cases. The side force values for case (2), is higher than ones of case (1) which indicates that the aerodynamic train design decreases the side force compared to the ordinary one at the same dimensions and the same angles of attack.

The side force values of case (2), is very close to the ones of case (3), despite the large velocities difference between them.es. The nature of the flow field and its structure depict by contours of velocity magnitude and streamline patterns along the train's cross-section has been also presented for different yaw angles. As can be seen from the stream line patterns along the train's cross-section, on the lower and upper leeward edges of the train a vortex is generated and grows steadily in the axial direction. An increase in the yaw angle results in an advance of the formation and breakdown of vortex on the leeward edges.

Contours of velocity magnitude were also computed for different yaw angles. The result showed that magnitude of rotating vortex in the leeward side pronounced with increasing yaw angle which leads to the creation of a low-pressure region in the lee ward side of the train causing high side force and roll moment. Obviously, the pressure distribution on the surface depends on the yaw angle. However, it does not change much along the train length except in a small region close to the nose. This shows that the pressure distribution around a high-speed train at higher yaw angles is almost independent on the axial position.

Generally, this study shows that unsteady CFD-RANS methods combined with an appropriate turbulence model can present an important means of assessing the crucial aerodynamic forces and moments of a high-speed train under strong crosswind conditions. Since the observed variations between some of the CFD and wind tunnel results may be due to the turbulence parameters such as turbulence intensity and length scale. The aerodynamic data obtained from this study can be used for comparison with future studies such as the influence of turbulent crosswinds on the aerodynamic coefficients of high-speed train moving in dangerous scenarios such as high embankments.

ACKNOWLEDGEMENT

We would like to express our sincere appreciation and gratitude to our supervisors: Prof. Dr. Ahmed Farouk Abdel Gawad and Prof. Dr. Mofreh Melad Nassef, for their supervision, guidance, encouragement and fruitful discussion.

REFERENCES

[1] Salleh, S. M., Ali, M. S. M., Salim, S. A. Z. S., Ishak, I. A., Shirakashi, M., & Muhammad, S. (2006). Aerodynamics characteristics around simplified high speed train model under the effect of crosswinds. ARPN J. Eng. Appl. Sci, 12.

[2] Correa, A. F. M. (2017). High-speed train aerodynamics under crosswinds: from standard wind tunnel testing to the effect of the train cooling systems.

[3] Kamal, M. N. F., Ishak, I. A., Darlis, N., Samiran, N. A., Mahmudin, R., Abd Rashid, R., ... & Khalid, A. (2019). Effect of Crosswind on Aerodynamic Characteristics of a Generic Train Model using ANSYS. Journal of Industry, Engineering and Innovation, 1(1).

[4] Ishak, I. A., Maruai, N., Sakri, F. M., Mahmudin, R., Samiran, N. A., Sulaiman, S., ... & Hassan, N. N. M. (2022). Numerical Analysis on the Crosswind Influence Around a Generic Train Moving on Different Bridge Configurations. Journal of Advanced Research in Fluid Mechanics and Thermal Sciences, 89(2), 76-

[5] Morden, J. A. (2017). A numerical investigation of the effects of crosswinds upon the aerodynamic characteristics of a high-speed passenger train and its slipstream (Doctoral dissertation, University of Birmingham).

[6] Khier, W., Breuer, M., & Durst, F. (2000). Flow structure around trains under side wind conditions: a numerical study. Computers & Fluids, 29(2), 179-195.

[7] Suzuki, M., Tanemoto, K., & Maeda, T. (2003). Aerodynamic characteristics of train vehicles under cross winds. Journal of wind engineering and industrial aerodynamics, 91(1-2), 209-218.

[8] Andersson, E., Häggström, J., Sima, M., & Stichel, S. (2004). Assessment of train-overturning risk due to strong cross-winds. Proceedings of the Institution of Mechanical Engineers, Part F: Journal of rail and rapid transit, 218(3), 213-223.

[9] Sanquer, S., Barre, C., de Virel, M. D., & Cleon, L. M. (2004). Effect of cross winds on high-speed trains: development of a new experimental methodology. Journal of Wind Engineering and Industrial Aerodynamics, 92(7-8), 535-545.

[10] Baker, C. J., & Sterling, M. (2009). Aerodynamic forces on multiple unit trains in cross winds. Journal of fluids engineering, 131(10).

[11] Thomas, D. (2009). Lateral stability of high-speed trains at unsteady crosswind (Doctoral dissertation, KTH Farkost & Flyg).

[12] Sakuma, Y., & Ido, A. (2009). Wind tunnel experiments on reducing separated flow region around front ends of vehicles on meter-gauge railway lines. Quarterly Report of RTRI, 50(1), 20-25.

[13] Dorigatti, F., Quinn, A. D., Sterling, M., & Baker, C. J. (2012). Evaluation of crosswind effects on rail vehicles through moving model experiments. In Proceedings of the Seventh International Colloquium on Bluff Body Aerodynamics and Applications (BBAA7) (pp. 2-6).

[14] Bouferrouk, A., Hargreaves, D., & Morvan, H. (2012, December). CFD simulations of crosswind impinging on a high-speed train model. In 18th Australasian Fluid Mechanics Conference, Launceston, Australia (pp. 3-7).

[15] Gilbert, T., Baker, C., & Quinn, A. (2013). Aerodynamic pressures around high-speed trains: the transition from unconfined to enclosed spaces. Proceedings of the Institution of Mechanical Engineers, Part F: Journal of Rail and Rapid Transit, 227(6), 609-622.

[16] Cui, T., Zhang, W., & Sun, B. (2014). Investigation of train safety domain in cross wind in respect of attitude change. Journal of Wind Engineering and Industrial Aerodynamics, 130, 75-87.

[17] Asress, M. B., & Svorcan, J. (2014). Numerical investigation on the aerodynamic characteristics of high-speed train under turbulent crosswind. Journal of Modern Transportation, 22(4), 225-234.

[18] Biadgo, A. M., Simonović, A., Svorcan, J., & Stupar, S. (2014). Aerodynamic characteristics of high-speed train under turbulent cross winds: A numerical investigation using unsteady-RANS method. FME Transactions, 42(1), 10-18.

[19] Flynn, D., Hemida, H., & Baker, C. (2016). On the effect of crosswinds on the slipstream of a freight train and associated effects. Journal of Wind Engineering and Industrial Aerodynamics, 156, 14-28.

[20] Correa, A. F. M. (2017). High-speed train aerodynamics under crosswinds: from standard wind tunnel testing to the effect of the train cooling systems.

[21] Yang, Y., Wang, X., Zhao, Y., Mao, J., & Xi, Y. (2017, April). Research on Motion Stability of High-Speed Trains under Cross-Wind Effect. In 2017 International Conference on Advanced Materials Science and Civil Engineering (AMSCE 2017) (pp. 70-74). Atlantis Press.

[22] Liu, T., Chen, Z., Zhou, X., & Zhang, J. (2018). A CFD analysis of the aerodynamics of a high-speed train passing through a windbreak transition under crosswind. Engineering Applications of Computational Fluid Mechanics, 12(1), 137-151.

[23] Gallagher, M., Morden, J., Baker, C., Soper, D., Quinn, A., Hemida, H., & Sterling, M. (2018). Trains in crosswinds–comparison of full-scale on-train measurements, physical model tests and CFD calculations. Journal of Wind Engineering and Industrial Aerodynamics, 175, 428-444.

[24] Niu, J., Zhou, D., & Liang, X. (2018). Numerical investigation of the aerodynamic characteristics of high-speed trains of different lengths under crosswind with or without windbreaks. Engineering Applications of Computational Fluid Mechanics, 12(1), 195-215.

[25] Yang, A. M., Zhang, C., Li, S. S., Zhang, L., Men, X. J., Kong, F. B., & He, S. Y. (2018). Numerical simulation on the aerodynamic performance of the high-speed train under crosswinds. Journal of Vibroengineering, 20(1), 550-572.

[26] Ishak, I. A., Ali, M. S. M., Sakri, F. M., Zulkifli, F. H., Darlis, N., Mahmudin, R. & Khalid, A. (2019). Aerodynamic Characteristics Around a Generic Train Moving on Different Embankments under the Influence of Crosswind.

[27] Yao, Z., Zhang, N., Chen, X., Zhang, C., Xia, H., & Li, X. (2020). The effect of moving train on the aerodynamic performances of train-bridge system with a crosswind. Engineering Applications of Computational Fluid Mechanics, 14(1), 222-235.

[28] LI HQ, Y. U. M. G., & ZHANG, Q. (2020). A numerical study of the aerodynamic characteristics of a high-speed train under the effect of crosswind and rain. Fluid Dynamics & Materials Processing, 16(1), 77-90.

[29] Wang, L., Luo, J., Li, F., Guo, D., Gao, L., & Wang, D. (2021). Aerodynamic performance and flow evolution of a high-speed train exiting a tunnel with crosswinds. Journal of Wind Engineering and Industrial Aerodynamics, 218, 104786.

[30] Zhang, L., Li, T., Zhang, J., & Piao, R. (2021). Optimization on the Crosswind Stability of Trains Using Neural Network Surrogate Model. Chinese Journal of Mechanical Engineering, 34(1), 1-17.

[31] Li, X., Tan, Y., Qiu, X., Gong, Z., & Wang, M. (2021). Wind tunnel measurement of aerodynamic characteristics of trains passing each other on a simply supported box girder bridge. Railway Engineering Science, 29(2), 152-162.

[32] Li, X., Chen, G., Krajnovic, S., & Zhou, D. (2021). Numerical Study of the Aerodynamic Performance of a Train with a Crosswind for Different Embankment Heights. Flow, Turbulence and Combustion, 107(1), 105-123.